Studying Bose/Fermi Systems in One Dimension with Continuous Matrix Product States

Clayton Peacock

December, 2019

1 Abstract

One can describe quantum systems in one spatial dimension through the use of continuous Matrix Product States (cMPS). It has been shown that cMPS can be used to model the quantum field equations of a one dimensional system of bosons and Fermions separately. This has been cross referenced successfully with analytical models such as the Bethe Ansatz. These findings were reproduced through performing computational optimization to find the ground state energies of various Bose/Fermi systems. cMPS were then used to explore the case of a Bose-Fermi mixture. Initial results agreed with expectation and this case continuous to be explored.

2 Introduction

I began my research with Dr. Carlos Bolech in the Summer of 2018, and we started by attempting to reproduce some of the findings of *continuous Matrix Product States for Quantum Fields* [1]. This was to be done by modeling a one dimensional system of composite particles, treated as bosons, using continuous

Matrix Product States (cMPS) [1] and using the Julia programming language [2]. This was previously done by a undergraduate researcher for Dr. Bolech using MatLab, and Julia appeared to be a much faster option for the project while still being a high-level environment similar to MatLab or Python. The creators of Julia describe the methods that they used to make Julia operate quickly as being: "Rich type information, provided naturally by multiple dispatch; Aggressive code specialization against run-time types; JIT compilation using the LLVM compiler framework" [2, 3].

3 General Theory

3.1 Optimization Problems

An optimization problem refers to a problem where an input vector is looked for which will either maximize or minimize the function which is to be optimized. An example of a simple two dimensional optimization problem is finding the minimum of the "Rosenbrock Function" [4] which is often used to exemplify and test different optimization packages and algorithms in computer programming. The optimization problems discussed in this paper will be minimization problems which utilize an algorithm to find the input vector which gives the lowest value for the energy function specified.

3.2 Variational Methods

In this paper, the minimization problem in question is to minimize the Hamiltonian of a molecule in its ground state. This type of optimization problem can be solved through variational methods, a popular example of which is the Ritz Method [5]. Variational methods are techniques which can be used to turn the solution of a problem into an optimization problem such as finding

the ground state energy of a molecule from its Hamiltonian [6]. One takes a "trial wave function" [6], calculates the expectation value of the Hamiltonian of the gas, and then simply needs to "tweak the parameters to get the lowest possible value" [6]. The normalized variational principal is given by Eq. (1) thus allows one to calculate an upper bound on the ground state energy [6]. In our case, we find the ground state energy specifically because this reflects the low temperature limit which gives the richest physics to analyze.

$$E_g \leq \langle \psi \mid H \mid \psi \rangle \equiv \langle H \rangle \tag{1}$$

One can sometimes compare these energy minima to exactly calculated values found through analytical techniques such as the Bethe Ansatz [7]. In many cases, the values cannot be exactly calculated, and in these cases cMPS can be used to gain more information about the system which would not be available otherwise.

3.3 Development of cMPS

The Numerical Renormalization Group (NRG) [8] and the Density Matrix Renormalization Group (DMRG) [9] were important to the development of models which simulate strongly correlated quantum systems [1]. The NRG and DMRG methods led to the development of Matrix Product States (MPS) that describe properties of 1-D quantum systems [1]. MPS in certain extensions of DMRG were then adapted by Verstraete and Cirac to describe quantum field theories in a model which they defined as "continuous Matrix Product States" (cMPS) [1].

3.4 cMPS Theory

A cMPS is described as "matrix product states in the continuum limit, without any reference to an underlying lattice parameter" [1]. The underlying MPS utilizes Singular Value Decomposition [10] in order to turn a vector of quantum amplitudes into a product of matrices representing the same quantum mechanical state [1]. This provides a path to model 1D lattice systems without needing to discretize the system [1]. A cMPS for a one dimensional system of bosons is defined as [1]:

$$\mid \chi\rangle = Tr_{aux}[\mathcal{P}e^{\int_0^L dx[Q(x)\otimes\hat{\mathbb{1}}+R(x)\otimes\hat{\psi}^\dagger(x)]}] \mid \Omega\rangle \tag{2}$$

4 Methods - Bosonic Case

To model the energy of bosons in one dimension, one takes cMPS expectation values of the field equations for the kinetic energy, interaction energy, and density of bosons. These equations can be coded using [1]:

$$\langle\chi \mid \chi\rangle = Tr(e^{TL}) \quad \text{with} \quad T = Q\otimes\mathbb{1}+\mathbb{1}\otimes\bar{Q}+R\otimes\bar{R} \tag{3}$$

$$\langle\partial_x\hat{\psi}_b^\dagger\partial_x\hat{\psi}_b\rangle = Tr[e^{TL}(iq_bR_b+[Q,R_b])\otimes(-iq_b\bar{R}_b+[\bar{Q},\bar{R}_b])] \tag{4}$$

$$\langle\hat{\psi}_b^\dagger\hat{\psi}_b^\dagger\hat{\psi}_b\hat{\psi}_b\rangle = Tr[e^{TL}(R_b^2\otimes\bar{R}_b^2)] \tag{5}$$

$$\langle\hat{\psi}_b^\dagger\hat{\psi}_b\rangle = Tr[e^{TL}(R_b\otimes\bar{R}_b)] \tag{6}$$

The Bosonic kinetic energy is given by Eq. (4), Eq. (5) gives the Bosonic interaction energy, and Eq. (6) gives the Bosonic density.

These equations are formulated using cMPS and include the matrices R and Q, which are chosen to be transitionally invariant and independent of x [1]:

$$Q(x) = Q \qquad R(x) = R \tag{7}$$

With D representing the bond dimension of an auxiliary space space, R is a $D \times D$ matrix which is free to be filled by an optimizer, and $R^\dagger R$ is diagonal [1]. For the construction of Q, a gauge can be partially fixed by imposing [1, 11]:

$$Q + Q^\dagger + R^\dagger R = 0 \tag{8}$$

This is possible because the state $\mid x\rangle$ is invariant under $Q \to XQX^{-1}, R \to XRX^{-1}$ and $Q \to Q + \alpha 1$[1]. Q is then a $D \times D$ matrix which is formulated by R and the matrix H_Q:

$$Q = iH_Q - \frac{1}{2}R^\dagger R \tag{9}$$

H_Q is a complex Hermitian matrix which is left free to be filled by the optimizer [1]. All quantities are well behaved in the thermodynamic limit $L \to \infty$ [1], and L was chosen to be high enough such that e^{TL} adopts its converged values. $L = 20$ was used for all runs as it is a high enough L such that e^{TL} is converged to the desired accuracy.

After constructing the equations in Julia, it was necessary to code the Hamiltonian "H", where "c" represents the interaction strength [1]:

$$H = \int_0^L dx \ (\partial_x \hat{\psi}_b^\dagger \partial_x \hat{\psi}_b + c \ \hat{\psi}_b^\dagger \hat{\psi}_b^\dagger \hat{\psi}_b \hat{\psi}_b) \tag{10}$$

The density was set to one using Lagrange multipliers. The following equation was added to the energy density function so that there would be a

large penalty (C_P) when the density was not one. C_P was chosen to be 10,000:

$$C_P(\langle\hat{\psi}_b^\dagger\hat{\psi}_b\rangle - 1)^2 \tag{11}$$

It was then necessary to find an optimal algorithm. Among the optimization packages available for use in Julia were Optim [12] and NLopt (NonLinear Optimization) [13]. Optim was chosen to explore first as it has the simpler syntax. Optim provided two algorithms that I compared at first: Nelder-Mead (a simplex algorithm) [14], and Simulated Annealing [15]. Optimizations using Simulated Annealing ran very slow and did not reach the necessary minima however Nelder-Mead was highly effective: converging quickly and accurately. NLopt was explored after updating to Julia 1.0. It was found that out of the many algorithms offered, PRAXIS [16] worked as well as Nelder-Mead in all cases. However, Nelder-Mead was used for all results because PRAXIS failed to find better minima in less time for any chosen c although it worked just as well. The code for the cMPS construction can be found in Appendix A.

5 Results - Bosonic Case

The previous findings [1] were reproduced quite successfully. The energy density graph "e(c) vs c" from [1] is shown in Fig. (1) and is to be compared to our findings in Fig. (2). Data was also collected on the run times as shown in Fig. (3).

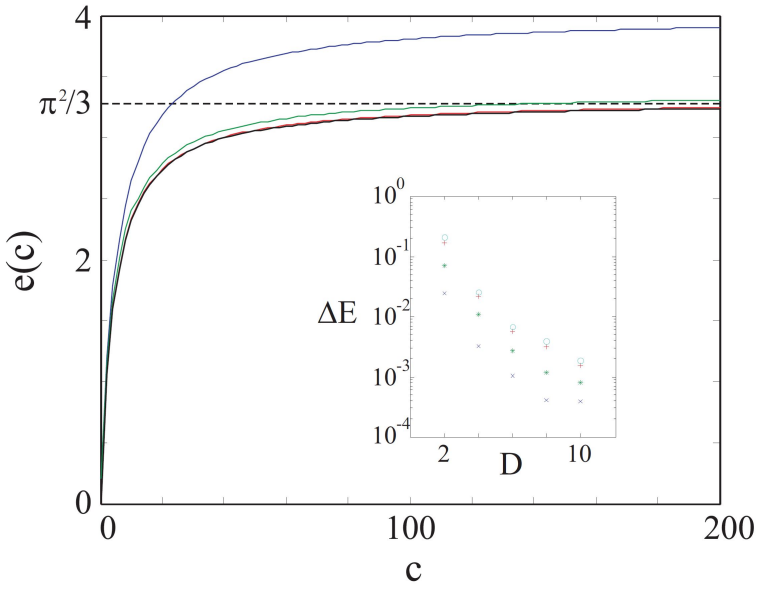

Figure 1: Energy Density as a function of interaction strength "c" for D = 2,4,6,8 from Fig 1 in [1]. The Bethe Ansatz results are plotted in black which is impossible to distinguish from the D=8 line in red [1]. This shows that as the bond dimension grows, cMPS grows more accurate

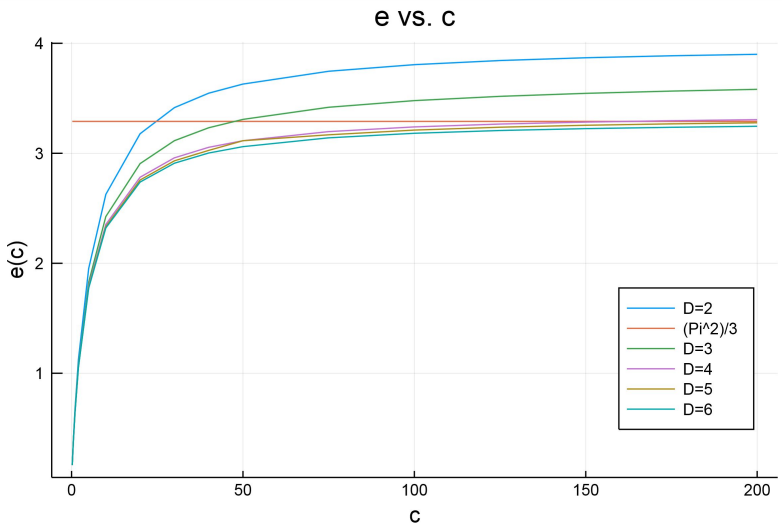

Figure 2: Energy density as a function of interaction strength "c" is plotted for our results using the Nelder-Mead algorithm. This was done for D=2,3,4,5,6 and the line $\pi^2/3$ was plotted as a reference point with Fig 1

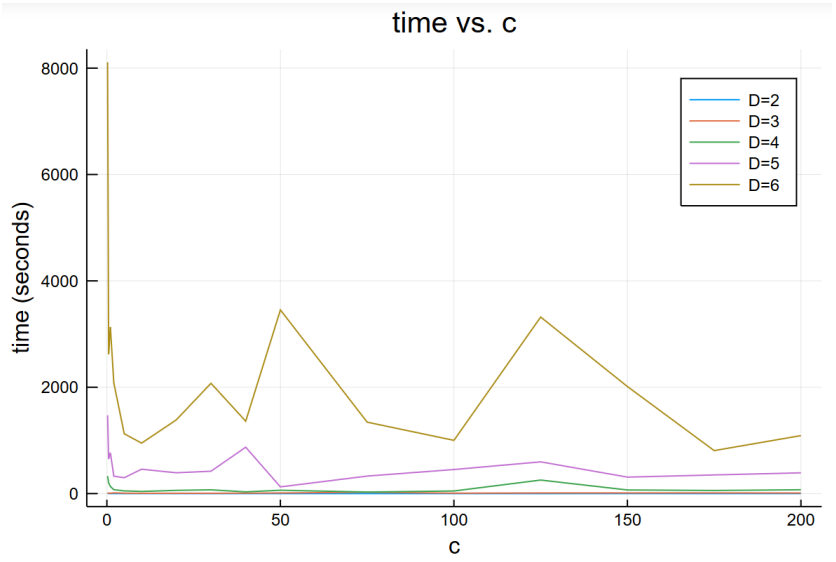

Figure 3: All runs were done on a laptop with 16 GB of RAM and the Processor: Intel(R) Core(TM) i7-7700HQ CPU @ 2.80GHz

6 Methods - Fermion Case

The next task was to reproduce results from *Matrix Product Ansatz for Fermi Fields in One Dimension* [17], which gives the general form for a "cMPS for spin-1/2 Fermions, for a system length of L and periodic boundary conditions [17, 18]:

$$\mid \chi\rangle = Tr_{aux}[\mathcal{P}e^{\int_0^L dx[Q(x)\otimes\hat{\mathbb{1}}+\Sigma_\sigma R_\sigma(x)\otimes\hat{\psi}^\dagger(x)]}] \mid \Omega\rangle \tag{12}$$

cMPS can be used to calculate the energy of spin-1/2 Fermions interacting through a contact potential, given by the Gaudin-Yang Hamiltonian [17, 19]:

$$H_{GY} = \int_0^L dx \sum_{\sigma=\uparrow,\downarrow} (\partial_x\hat{\psi}^\dagger_\sigma\partial_x\hat{\psi}_\sigma - 2\Delta\hat{\psi}^\dagger_\sigma\hat{\psi}^\dagger_{\bar{\sigma}}\hat{\psi}_{\bar{\sigma}}\hat{\psi}_\sigma) \tag{13}$$

Our model was tested with Δ set to one. The cMPS equations for energies and density are again made up of complex matrices [17]. However, now it was necessary to introduce two complex matrices $R_\uparrow$ and $R_\downarrow$ representing up and down spin Fermions [17]. These are referred to succinctly as R_σ with sigma being up or down. $R_\uparrow$ and $R_\downarrow$ are in principle free to be filled by the optimizer, and Q is chosen using the cMPS gauge freedom as before [17, 1, 11]:

$$Q = iH_Q - \frac{1}{2}R^\dagger_\uparrow R_\uparrow - \frac{1}{2}R^\dagger_\downarrow R_\downarrow \tag{14}$$

Here, H_Q is a complex Hermitian matrix [17], formulated in the same way as in the Bosonic case. The Q matrix is taken to be independent of coordinates however R_σ is allowed to have a phase modulation upon it [17]:

$$Q(x) = Q \qquad R_\sigma(x) = R_\sigma e^{iq_\sigma x} \tag{15}$$

q_σ is a pair of real variational parameters [17]. T is translationally invariant and given by [17]:

$$T(x) \equiv Q(x) \otimes \mathbb{1} + \mathbb{1} \otimes \bar{Q}(x) R_\uparrow(x) + R_\downarrow(x) \otimes \bar{R}_\downarrow(x) + R_\uparrow(x) \otimes \bar{R}_\uparrow(x) \equiv T \quad (16)$$

Finally, the quantum field equations are all independent of x [17], and $\bar{\sigma}$ represents the opposite spin of σ in the cMPS expectation values of the field equations given below [17]:

$$\langle \partial_x \hat{\psi}_\sigma^\dagger \partial_x \hat{\psi}_\sigma \rangle = Tr[e^{TL}(iq_\sigma R_\sigma + [Q, R_\sigma]) \otimes (-iq_\sigma \bar{R}_\sigma + [\bar{Q}, \bar{R}_\sigma])] \quad (17)$$

$$\langle \hat{\psi}_\sigma^\dagger \hat{\psi}_{\bar{\sigma}}^\dagger \hat{\psi}_{\bar{\sigma}} \hat{\psi}_\sigma \rangle = Tr[e^{TL}(R_\sigma R_{\bar{\sigma}} \otimes \bar{R}_\sigma \bar{R}_{\bar{\sigma}})] \quad (18)$$

$$\langle \hat{\psi}_\sigma^\dagger \hat{\psi}_\sigma \rangle = Tr[e^{TL}(R_\sigma \otimes \bar{R}_\sigma)] \quad (19)$$

Lagrange multipliers were ineffective at implementing the physical constraints for the Fermion case [17]:

$$\{R_\uparrow, R_\downarrow\} = 0 \qquad \text{and} \qquad R_\sigma^2 = 0 \quad (20)$$

In the Bosonic case, Lagrange multipliers worked well because the density is a singular constant number. However in the Fermi case the constraints deal with matrices, and no formulation of Lagrange multipliers were successful. Therefore, an algebraic implementation of the constraints through a different construction of $R_\uparrow$ and $R_\downarrow$ was used [17].

In order to satisfy the constraints, $R_\uparrow$ was chosen to have a Jordan canonical

form [17, 20]:

$$R_{\uparrow} = \begin{pmatrix} 0 & \mathbb{I} \\ 0 & 0 \end{pmatrix} \tag{21}$$

$R_{\downarrow}$ was constructed out of two real $D/2 \times D/2$ matrices A and B which were to be filled by the optimizer [17]. Invertible, complex, $D/2 \times D/2$ "P" matrices were introduced around our construction of $R_{\downarrow}$ which the optimizer was free to fill to set $R_{\downarrow}$ to the same Jordan form as $R_{\uparrow}$ [17]. :

$$R_{\downarrow} = \begin{pmatrix} A & B \\ 0 & -A \end{pmatrix} \tag{22}$$

In the Fermi case, the free energy is minimized and created from the energy density $\hat{H}_{GY}/L$ and a combination of the chemical potential μ, the magnetic field h, and the densities $n_{\uparrow}$ and $n_{\downarrow}$ [17]. The zero-temperature free-energy operator is given by (23) [17].

$$\hat{f} = \hat{H}_{GY}/L - \mu(\hat{n}_{\uparrow} + \hat{n}_{\downarrow}) - h(\hat{n}_{\uparrow} - \hat{n}_{\downarrow}) \tag{23}$$

There were no constraints on the densities in this case [17]. μ and h were chosen such that each minimization run cycled through the grey path in Fig 4 [17] which was parameterized with a single angle [17, 21]: The angle was varied from $-60°$ to $200°$, ignoring the vacuum cases in which the ground state is trivial [17]. The Nelder-Mead algorithm [14] in the Optim package [12] achieved the same minima as PRAXIS [16] in the NLopt package [13] for many of the higher angles above $60°$ and converged well for the lower angles where no other algorithm showed good convergence. Therefore, Nelder-Mead was used for all runs as it was in the Bosonic case. However, subsequent runs were started by using a previous angle's successful minimizing vector as a starting vector for the next angles (as was done with the Bosonic case), and it was found that PRAXIS

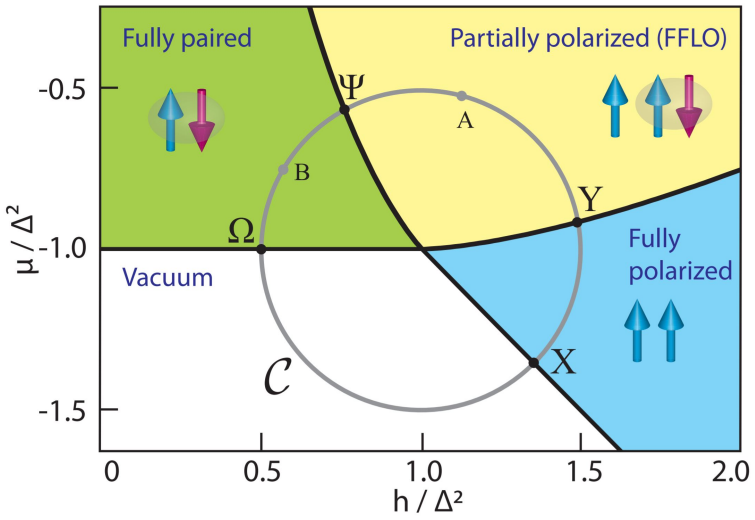

Figure 4: Fig 2 from *Matrix Product Ansatz for Fermi Fields in One Dimension* [17]

finds a better initial minimizer starting from a random initial vector more often than Nelder-Mead. Thus PRAXIS was used to find the first minimizer, and Nelder-Mead was then used to find all other angles. This saved processing time and improved accuracy when compared to using random starting vectors for every angle.

7 Results - Fermion Case

Our results for the lower angles up to 25° are very consistent with the previous results [17] as shown in Fig. (5). This corresponds to the fully polarized section of Fig. (4) [2]. For other angles, our free energy minima were higher than those of previous cMPS results of one-dimensional gases [17]. This could be due to a number of reasons. One possible reason is that the findings of [17] were determined using the Simulated Annealing [15] and Gradient Descent [22] algorithms for which the gradient was numerically determined by the optimizer.

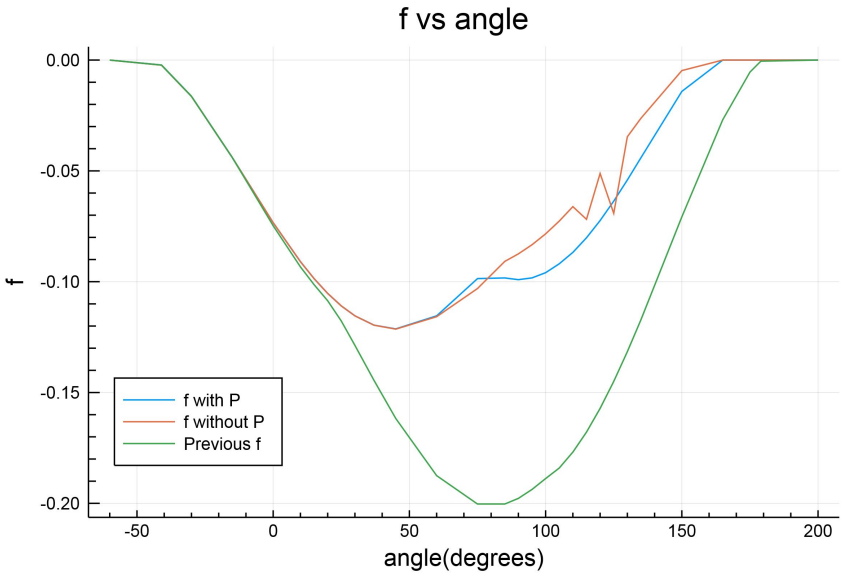

Figure 5: Results are included for cases with and without P matrices implemented to show how they impact results. D=8 results are shown for both our data and previous data.

In addition, our results may become more accurate with increasing D above $D = 8$. However, $D = 12$ was not tried because it did not converge easily when tried before by Dr. Sangwoo Chung and there was initial difficulty with converging $D = 16$ on our equipment in a timely manner. Finally, the densities were graphed in order to compare with the densities found in [2] (see Fig. (6).

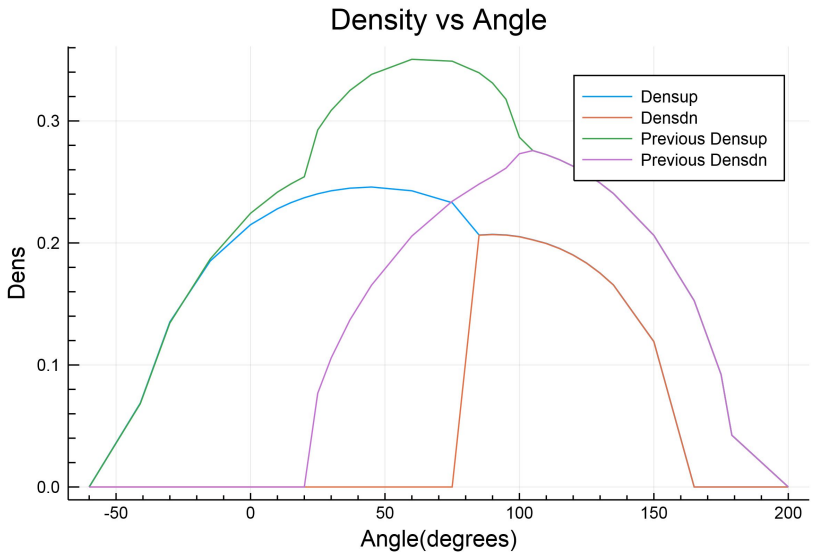

Figure 6: Here, $n_\uparrow$ agrees fairly with previous data in [2], but $n_\downarrow$ drops off sharply at 85°.

8 Color Superconductivity in FFLO States

Superconductivity describes states in which electric resistance goes to zero as temperature drops below a critical value T_c [23]. According to BCS theory (1964) [24]; electrons (fermions) near the Fermi surface form Cooper-pairs [25]. These Cooper-pairs, consisting of two fermions, will then act as bosons. At sufficiently low temperatures (below T_c) these bosons can form a Bose-Einstein condensate which causes the state to become superconducting [24].

In high-field superconductors, "Fermi surfaces corresponding to electrons with opposite spins" can be separated by a strong magnetic field which is "coupled to the spins of the conduction electrons" [23]. Pairing is destroyed if the surfaces are separated by too large of a distance, and the superconducting state becomes less favorable than the normal one. Close to this transition line, it has been shown [26][27] that a new state is formed, called the FFLO (or LOFF) phase [23]. Thus, under a high magnetic field, superconducting states are de-

scribed by FFLO (or LOFF) theory [26][27]. FFLO states can be achieved in ultra cold atomic gases and then predicted and analysed using cMPS (see Fig. (4) for angles $25° - 115°$).

In addition, quark Cooper-pairing has been theorized to occur in highly dense quark matter [28] [29]. In quark superfluids of high densities, diquark condensates can form as Cooper-pairs which then experience Bose-Einstein condensation at sufficiently low temperatures [23]. These diquarks break color-gauge symmetry and their Bose-Einstein condensation leads to the phenomena known as color-superconductivity [23]. It is theorized that quark matter can undergo Bose-Einstein condensation in highly-dense, cold, astrophysical objects [29]. Currently, neutron stars are the most likely candidate to have color-superconducting states at their core [29].

When a massive star dies, it exploding away some of its mass in a supernova and the remainder of the star collapses down into a highly compact and dense core of nucleons called a neutron star [30]. In their core neutron stars are theorized to have quark matter held at high density. Furthermore, neutron stars have strong magnetic fields [30] and thus neutron stars are likely to contain FFLO states of color-superconductivity [29]. These states are expected to be analogous of FFLO states in ultracold atomic gases. Therefore using cMPS to effectively describe and explore FFLO states in an ultracold atom context could lead to a greater understanding of color-superconducting states in the core of neutron stars.

9 Methods - Bose-Fermi Mixture Case

For the mixture case, the Bosonic and Fermionic kinetic energies were needed as well as the Bosonic interaction (5) and the Bose-Fermi densities ((6) and (19) respectively) [31]. It was also necessary to introduce the field equations

for Bose-Fermi interaction [31]:

$$\begin{aligned}\langle\hat{\psi}_b^\dagger\hat{\psi}_f^\dagger\hat{\psi}_f\hat{\psi}_b\rangle &= Tr\{e^{TL}(R_bR_f\otimes\mathbb{1})\cdot(\mathbb{1}\otimes\bar{R}_b\bar{R}_f)\} \\ &= Tr\{e^{TL}(R_bR_f\otimes\bar{R}_b\bar{R}_f\}\end{aligned} \tag{24}$$

The problem was kept simpler by assuming all Fermi particles would be of the same spin. Thus there can not be a contact Fermi interaction term because of the consequences of the Pauli-Exclusion Principle [32]. Finally, the energy function for the mixtures case as given in [31] is:

$$\begin{aligned}H = &\int_0^L dx(\frac{\hbar^2}{2m_b}\partial_x\hat{\psi}_b^\dagger\partial_x\hat{\psi}_b + \frac{\hbar^2}{2m_f}\partial_x\hat{\psi}_f^\dagger\partial_x\hat{\psi}_f) \\ &+ \int_0^L dx(\frac{1}{2}g_{bb}\hat{\psi}_b^\dagger\hat{\psi}_b^\dagger\hat{\psi}_b\hat{\psi}_b + g_{bf}\hat{\psi}_b^\dagger\hat{\psi}_f^\dagger\hat{\psi}_f\hat{\psi}_b)\end{aligned} \tag{25}$$

The mixtures case is like the Fermi case in that it will have two R matrices, now R_b and R_f rather than $R_\uparrow$ and $R_\downarrow$ [31]. In addition, new constraints need to be satisfied [31]:

$$[R_b, R_f] = 0 \qquad \text{and} \qquad R_f^2 = 0 \tag{26}$$

In addition, q_b and q_f will be included similar to $q_\uparrow$ and $q_\downarrow$ [31]. The interaction strengths and masses will be set equal to begin: $g_{bb} = g_{bf} = g$ and $m_b = m_f = m$. Once results are found to consistently and accurately match exact values we will begin to vary g and explore novel physics of one-dimensional Bose/Fermi mixtures.

10 Results - Bose-Fermi Mixture Case

Results were found for the Bose/Fermi mixture cases with g = 2, g = 50, and g = 100, each for D = 2, 4, and 6 excluding the g = 2 case for D = 2 which is currently being explored. In each of these cases, the total density is set at a constant value of $n_b + n_f = 0.25$ with the plots showing the fermion density varied from 0 to 0.23 on the horizontal axis. The vertical axis shows the energy density "e" where $e = (2 \times E)/n_t^3$ where E is the ground energy found through optimization and n_t is the total density. All results were found with the PRAXIS algorithm [16] and the cases are plotted in Figures (7),(8), and (9). The results show that energy density tends to decrease as the Bond-dimension (D) increases, which is expected and can be explicitly seen in Fig. (10). The trends of our data also match the trends of the Bethe Ansatz values, particularly for D = 6. Compared to the exact values, D = 4 results have an average $15-25\%$ error while D = 6 results have an average $5-10\%$ error. Preliminary results have been found for D = 8 for which the energy density is lower than D = 6 values but higher than Bethe Ansatz values, reducing the error to 4%. These results look promising and cases of $D > 8$ will continue to be explored. Once it is verified that $D > 8$ cases behave as expected, novel physics can be explored in Bose/Fermi mixtures.

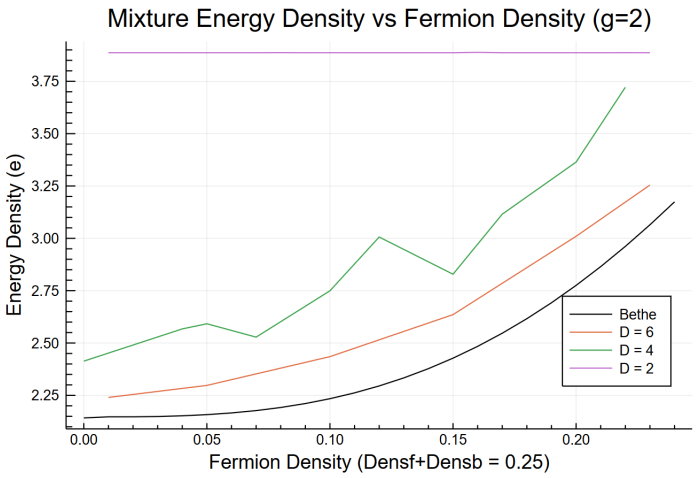

Figure 7: Mixture Case Results for g = 2

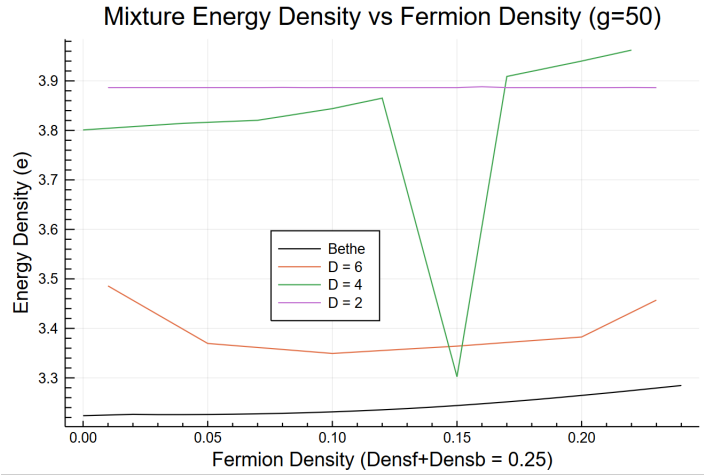

Figure 8: Mixture Case Results for g = 50

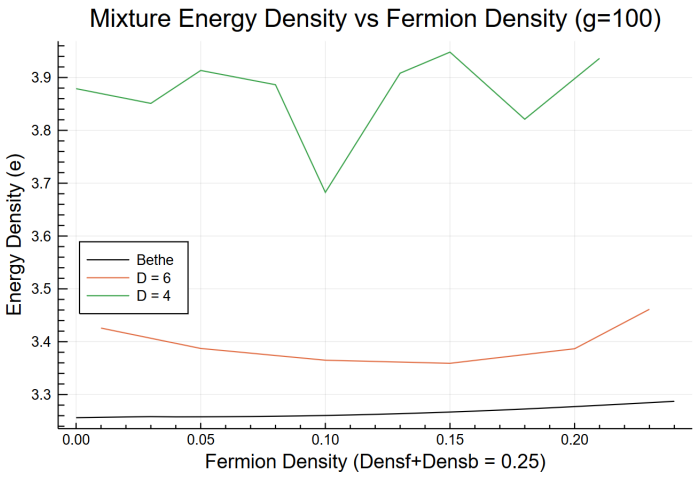

Figure 9: Mixture Case Results for g = 100

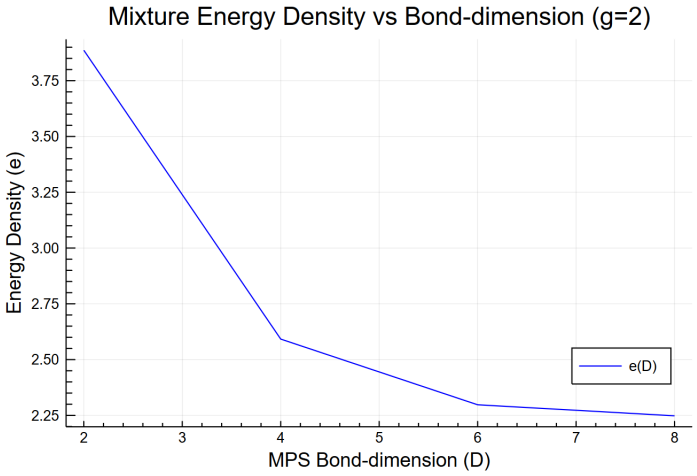

Figure 10: Energy Density (e) vs Bond-dimension (D)

11 Conclusion

In conclusion, Continuous Matrix Product States provide an accurate and effective way to describe quantum field theories, and have the potential to further our understanding of ultracold atom systems of many kinds. In addition, effectively using cMPS to explore FFLO states in one-dimensional Fermi gases has the potential to further research of analogous FFLO states reached in highly compact astrophysical objects such as neutron stars. The findings of [1] were successfully reproduced to within a small margin. In the Fermionic case the findings of the free-energy [17] were reproduced very accurately in the range of angles $-60°$ to $25°$. From angles $25°$ to $200°$ the findings were much less accurate. At this point it was deemed more fruitful to move on to the mixtures case, however the Fermionic case will be revisited. In the mixtures case, initial results come close to exact Bethe Ansatz values, with increasing D converging to increasingly lower values above the Bethe Ansatz results. Bond dimensions higher than D = 6 will continue to be explored and eventually cMPS will be used to explore further physics such as a Bose/Fermi mixture with differing interaction strengths and masses ($g_bf \neq g_bb, m_f \neq m_b$). [33] [34]

References

[1] F. Verstraete and J. I. Cirac. Continuous matrix product states for quantum fields. *Phys. Rev. Lett.*, 104:190405, May 2010.

[2] JuliaLang.org contributors. The julia programming language.

[3] Chris Lattner and Vikram Adve. Llvm: A compilation framework for lifelong program analysis & transformation. In *Proceedings of the International Symposium on Code Generation and Optimization: Feedback-directed and Runtime Optimization*, CGO '04, pages 75–, Washington, DC, USA, 2004. IEEE Computer Society.

[4] Eric W. Weisstein. 'rosenbrock function' from mathworld–a wolfram web resource.

[5] J. K. L. MacDonald. Successive approximations by the rayleigh-ritz variation method. *Phys. Rev.*, 43:830–833, May 1933.

[6] David J. Griffiths. *Introduction to Quantum Mechanics*. Prentice Hall, 1994.

[7] Michael Karbach and Gerhard Muller. Introduction to the Bethe ansatz I. *arXiv e-prints*, pages cond–mat/9809162, Sep 1998.

[8] Kenneth G. Wilson. The renormalization group: Critical phenomena and the kondo problem. *Rev. Mod. Phys.*, 47:773–840, Oct 1975.

[9] Steven R. White. Density matrix formulation for quantum renormalization groups. *Phys. Rev. Lett.*, 69:2863–2866, Nov 1992.

[10] Eric W. Weisstein. 'singular value decomposition' from mathworld–a wolfram web resource.

[11] Jutho Haegeman, J. Ignacio Cirac, Tobias J. Osborne, and Frank Verstraete. Calculus of continuous matrix product states. *Phys. Rev. B*, 88:085118, Aug 2013.

[12] Patrick Kofod Mogensen and Asbjørn Nilsen Riseth. Optim: A mathematical optimization package for Julia. *Journal of Open Source Software*, 3(24):615, 2018.

[13] Steven G. Johnson. The nlopt nonlinear-optimization package.

[14] J. A. Nelder and R. Mead. A Simplex Method for Function Minimization. *The Computer Journal*, 7(4):308–313, 01 1965.

[15] P.J.M. Laarhoven, van and E.H.L. Aarts. *Simulated annealing : theory and applications*. Mathematics and its applications. Reidel, 1987.

[16] Karl R. Gegenfurtner. Praxis: Brent's algorithm for function minimization. *Behavior Research Methods, Instruments, & Computers*, 24(4):560–564, Dec 1992.

[17] Sangwoo S. Chung, Kuei Sun, and C. J. Bolech. Matrix product ansatz for fermi fields in one dimension. *Phys. Rev. B*, 91:121108, Mar 2015.

[18] Jutho Haegeman, J. Ignacio Cirac, Tobias J. Osborne, Henri Verschelde, and Frank Verstraete. Applying the variational principle to (1 + 1)-dimensional quantum field theories. *Phys. Rev. Lett.*, 105:251601, Dec 2010.

[19] M. Gaudin. Un systeme a une dimension de fermions en interaction. *Physics Letters A*, 24(1):55 – 56, 1967.

[20] Roger A. Horn and Charles R. Johnson. *Matrix Analysis*. Cambridge University Press, New York, NY, USA, 2nd edition, 2012.

[21] G. Orso. Attractive fermi gases with unequal spin populations in highly elongated traps. *Phys. Rev. Lett.*, 98:070402, Feb 2007.

[22] Sebastian Ruder. An overview of gradient descent optimization algorithms. *CoRR*, abs/1609.04747, 2016.

[23] Roberto Casalbuoni and Giuseppe Nardulli. Inhomogeneous superconductivity in condensed matter and qcd. *Rev. Mod. Phys.*, 76:263–320, Feb 2004.

[24] J. Bardeen, L. N. Cooper, and J. R. Schrieffer. Theory of superconductivity. *Phys. Rev.*, 108:1175–1204, Dec 1957.

[25] Michael Tinkham. *Introduction to Superconductivity.* Dover Publications, 2 edition, June 2004.

[26] Peter Fulde and Richard A. Ferrell. Superconductivity in a strong spin-exchange field. *Phys. Rev.*, 135:A550–A563, Aug 1964.

[27] A. I. Larkin and Y. N. Ovchinnikov. Nonuniform state of superconductors. *Zh. Eksp. Teor. Fiz.*, 47:1136–1146, 1964. [Sov. Phys. JETP20,762(1965)].

[28] D. D. Ivanenko and D. F. Kurdgelaidze. Quark stars. *Soviet Physics Journal*, 13(8):1015–1019, Aug 1970.

[29] Mark G. Alford, Andreas Schmitt, Krishna Rajagopal, and Thomas Schäfer. Color superconductivity in dense quark matter. *Rev. Mod. Phys.*, 80:1455–1515, Nov 2008.

[30] D. Maoz. *Astrophysics in a Nutshell.* In a Nutshell. Princeton University Press, 2007.

[31] Adilet Imambekov and Eugene Demler. Exactly solvable case of a one-dimensional bose–fermi mixture. *Phys. Rev. A*, 73:021602, Feb 2006.

[32] Daniel V. Schroeder. *An introduction to thermal physics*. Pearson, 2014.

[33] S. S. Chung, S. Bauman, Kuei Sun, and C. J. Bolech. On the new continuous matrix product ansatz. *Journal of Physics: Conference Series*, 702:012004, mar 2016.

[34] Sangwoo S. Chung and C. J. Bolech. Multiple phase separation in one-dimensional mixtures of mass- and population-imbalanced attractive fermi gases. *Phys. Rev. A*, 96:023609, Aug 2017.

12 Appendix A - Bosonic cMPS code

```
using Optim
using LinearAlgebra
const D = 8 #choosing bond dimension
const c = 2 #choosing interaction strength
const L = 2
function Ec(x::Vector)
    R = reshape(Complex.(x[1:2:2*D^2-1],x[2:2:2*D^2]),D,D)
    H = reshape(x[2*D^2+1:3*D^2],D,D)
    H = Hermitian(Complex.(H,LowerTriangular(H)'-Diagonal(H)))
    Q = - im*H - 0.5*(R'*R)
    T = kron(Q,Diagonal(ones(D))) +
        kron(Diagonal(ones(D)),conj(Q)) +
        kron(R,conj(R))

    ExpT = exp(T)
    ExpTL = ExpT^L
```

```
    epsilon = norm(ExpTL-ExpT,1)/1_000_000
    while norm(ExpTL-ExpT,1) > epsilon
        ExpT = ExpTL
        ExpTL = ExpT^2
    end

    commutator(A,B) = A*B - B*A
    commQR = commutator(Q,R)

    Ekin = tr(ExpTL * kron(commQR,conj(commQR)))
    Eint = tr(ExpTL * kron(R^2,conj(R^2)))
    Dens = tr(ExpTL * kron(R,conj(R)))

    e_c = (Ekin+c*Eint)/Dens + 10_000*(Dens-1.0)^2

    return  real(e_c)
end

const Sigma=D
x0=randn(3*D^2)/Sigma
@time results= optimize(Ec,x0
    , NelderMead(), Optim.Options(iterations =
    100000);autodiff=:forward)
```